Journal of Process Control 28 (2015) 27–39

Contents lists available at ScienceDirect

Journal of Process Control

journal homepage: www.elsevier.com/locate/jprocont

Diagnosis of multiple and unknown faults using the causal map and multivariate statistics

Leo H. Chiang[a,b], Benben Jiang[c,d], Xiaoxiang Zhu[c], Dexian Huang[d], Richard D. Braatz[a,c,*]

[a] Department of Chemical and Biomolecular Engineering, University of Illinois at Urbana-Champaign, Urbana, IL 61801, USA
[b] Dow Chemical Company, Texas Operations, 2301 Brazosport Blvd., Freeport, TX 77541, USA
[c] Department of Chemical Engineering, Massachusetts Institute of Technology, Cambridge, MA 02139, USA
[d] Department of Automation, Tsinghua University and Tsinghua National Laboratory for Information Science and Technology, Beijing 100084, China

ARTICLE INFO

Article history:
Received 29 August 2014
Received in revised form 25 January 2015
Accepted 20 February 2015
Available online 13 March 2015

Keywords:
Fault diagnosis
Feature extraction
Feature representation
Multiple faults
Unknown faults
Process monitoring
Chemometrics
Causal map
Multivariate statistics

ABSTRACT

Feature extraction is crucial for fault diagnosis and the use of complementary features allows for improved diagnostic performance. Most of the existing fault diagnosis methods only utilize data-driven and causal connectivity-based features of faults, whereas the important complementary feature of the propagation paths of faults is not incorporated. The propagation path-based feature is important to represent the intrinsic properties of faults and plays a significant role in fault diagnosis, particularly for the diagnosis of multiple and unknown faults. In this article, a three-step framework based on the modified distance (DI) and modified causal dependency (CD) is proposed to integrate the data-driven and causal connectivity-based features with the propagation path-based feature for diagnosing known, unknown, and multiple faults. The effectiveness of the proposed approach is demonstrated on the Tennessee Eastman process.

1. Introduction

Feature extraction is a process that builds derived values (features) from an initial set of information to inform and facilitate the desired task, in some cases leading to better human interpretations. Feature extraction is crucial for fault diagnosis. Extraction of features that can fully reflect the intrinsic properties of the faults, especially the unknown and multiple faults, is still a challenging problem. This issue has not been extensively explored in fault monitoring, in contrast to the high level of achievement in pattern recognition and image processing [1].

The purpose of fault diagnosis is to determine the root causes of process faults, which facilitates efficient, safe, and optimal operation of industrial processes [2]. The chemical industry mostly constructs process monitoring systems based on process data, and several reviews on fault diagnosis based on data-driven feature extraction are available [3–8]. Those fault diagnosis methods typically do not utilize the preliminary process knowledge. The traditional techniques purely based on historical process data have an inherent limitation for diagnosing multiple faults. Multiple faults can be defined as two or more faults occur simultaneously or sequentially, which can be categorized as being of four types: induced fault, independent multiple faults, masked multiple faults, and dependent faults [9], as shown in Fig. 1. The joint effect on overlapping variables can be very different than the effect of the individual faults. In those data-driven diagnosis techniques, a few variables are isolated as the candidates for the likely root cause of the faults. In large-scale plants with high complexity, it is difficult to conclude whether a certain variable is the root cause by analyzing plant data alone [10,11].

To address this drawback, the feature representation of causal connectivity of the components within the plant is considered and several ways of combining data-driven techniques with cause-and-effect information from a process flow diagram or piping and instrumentation diagram have been carried out. Lee et al. [9] utilized a hybrid method of signed digraph and partial least squares for the fault diagnosis of chemical processes. Using the local qualitative relationships of each variable in a signed digraph, a process is decomposed into subprocesses. A partial least-squares model is then built for the estimation of each measured variable in each decomposed subprocess. Alternately, Thornhill et al. [12] showed

* Corresponding author at: 77 Massachusetts Avenue, Room E19-551, Cambridge, MA 02139, USA. Tel.: +1 617 253 3112; fax: +1 617 258 5042.
E-mail address: braatz@mit.edu (R.D. Braatz).

http://dx.doi.org/10.1016/j.jprocont.2015.02.004
0959-1524/

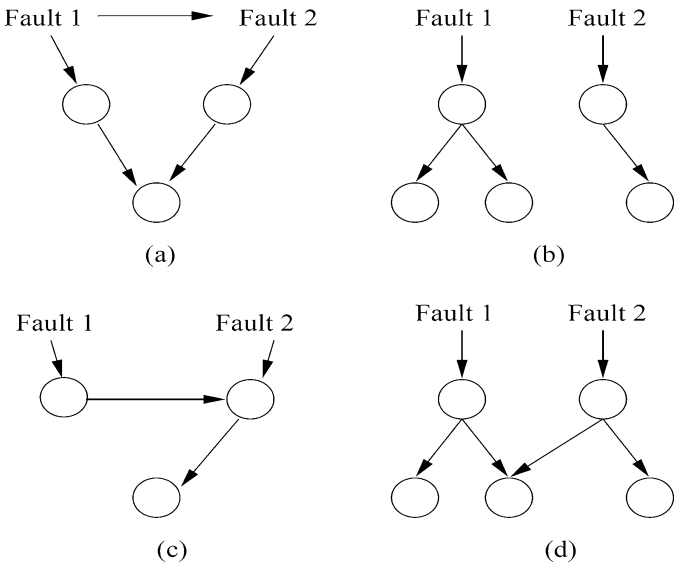

Fig. 1. Four types of multiple faults: (a) induced faults, (b) independent faults, (c) masked multiple faults, and (d) dependent multiple faults. A node represents a symptom and a vector represents the causal relationship between two nodes.

how data-driven methods in combination with cause-and-effect relationships among process variables could lead to efficient root cause diagnosis, where the root cause of a plant-wide oscillatory disturbance was determined, and its means of propagation understood. More recently, Thambirajah et al. [13] also developed an approach that combines the data-driven technique of transfer entropy with a technique that uses the cause-and-effect information in the plant schematic in the form of a connectivity matrix. The core technology for the extraction of a connectivity matrix is an XML code of the chemical plant that represents the items of equipment and the links between them.

Aside from the feature extractions from data-driven and causal map techniques, the propagation path of a fault is another important feature for representing the intrinsic properties of faults. As shown in Fig. 1, different faults often have their own distinctive dynamic propagation among process variables. Such information plays a significant role in fault diagnosis, particularly for the diagnosis of multiple and unknown faults. The feature of fault propagation path is significantly different from the aforementioned two feature representations extracted from plant data and causal connectivity (DI and CD, respectively), and can effectively complement them to allow better diagnostic performance. It was shown in [14] that the information provided by different feature representations can be complementary and the use of complementary features greatly improves diagnosis performance.

This study proposes a scheme that incorporates more complete feature representations for fault diagnosis. Previously, the authors introduced the modified distance (DI) and modified causal dependency (CD) to incorporate the data-driven approach in conjunction with the causal connectivity-based approach for detecting and identifying faults [16]. The DI is based on the Kullback–Leibler information distance (KLID), the mean of the measured variables, and the range of the measured variables. The CD is derived based on the multivariate T^2 statistic. This article presents an approach based on the DI/CD that systematically utilizes a more complete set of feature representations, including the data-driven, causal connectivity-based, and propagation path-based features, for diagnosing known, unknown, and multiple faults.

The rest of this article is organized as follows. Section 2 describes the DI/CD-based algorithm for diagnosing known, unknown, and multiple faults. The proposed method is evaluated in Section 3 using data sets from a chemical plant simulator for the Tennessee Eastman Process. Section 4 summarizes the conclusions.

2. Methods

2.1. Modified distance and modified causal dependency

The modified distance (DI) and modified causal dependency (CD), which serve as the basis of the proposed diagnosis method for multiple and unknown faults, are briefly reviewed in this section. More details of the two techniques can be found in [16].

The DI is based on the Kullback–Leibler information distance (KLID), the mean of the measured variables, and the range of the measured variable. The DI is used to measure the similarity of the measured variable between the current operating condition and historical operating conditions. When the DI is larger than the predefined threshold, the variable is identified as abnormal with respect to the historical operating conditions. The KLID for the historical distribution of the variable q is defined by

$$f_{h,t}^{q} := I(p_{h,t}^{q}, 1) \tag{1}$$

where the historical distribution $p_{h,t}^{q}$ is constructed for data collected from time $t-b+1$ to t (b is the window size), $I(p_1, p_2) := \int p_1(x)\ln(p_1(x)/p_2(x))dx$ where $p_1(x)$ and $p_2(x)$ are two distributions, and the integral is calculated numerically. When $p_{h,t}^{q}$ is the uniform distribution, the value of $f_{h,t}^{q}$ is equal to zero.

With $f_{\bar{h},t}^{q}$ defined as the KLID of the historical distribution computed by using all n observations, the absolute difference between the current KLID $f_{r,t}^{q}$ and historical KLID $f_{\bar{h},t}^{q}$ for a fault is calculated as

$$\widetilde{f}_{r,t}^{q} := \left| f_{r,t}^{q} - f_{\bar{h},t}^{q} \right|. \tag{2}$$

Similarly, the absolute difference between the current mean $m_{r,t}^{q}$ and historical mean $m_{\bar{h},t}^{q}$ is

$$\widetilde{m}_{r,t}^{q} := \left| m_{r,t}^{q} - m_{\bar{h},t}^{q} \right| \tag{3}$$

and the absolute difference between current range $s_{r,t}^{q}$ and historical range $s_{\bar{h},t}^{q}$ is

$$\widetilde{s}_{r,t}^{q} := \left| s_{r,t}^{q} - s_{\bar{h},t}^{q} \right| \tag{4}$$

where the mean and the range of the variable q at current time $t=T$ is

$$m_{r,t}^{q} := \frac{1}{b}\sum_{t=T-b+1}^{T} q_t \tag{5}$$

and

$$s_{r,t}^{q} := \max_{T-b+1\le t\le T} q_t - \min_{T-b+1\le t\le T} q_t \tag{6}$$

respectively.

The normalized KLID associated with the recent distribution and the historical distribution for the fault is defined by

$$F_{r,t}^{q} := \frac{\widetilde{f}_{r,t}^{q}}{\mathrm{mean}(\widetilde{f}_{h,t}^{q}) + n_r \mathrm{std}(\widetilde{f}_{h,t}^{q})} \tag{7}$$

where n_r is a constant used to specify the misclassification error (type-I error) which can be determined based on the historical data. A similar recent distribution and the historical distribution will result in $F_r^q < 1$.

The normalized mean is

$$M_{r,t}^q := \frac{\tilde{m}_{r,t}^q}{\text{mean}(\tilde{m}_{h,t}^q) + n_r \text{std}(\tilde{m}_{h,t}^q)} \tag{8}$$

and the normalized range is

$$S_{r,t}^q := \frac{\tilde{s}_{r,t}^q}{\text{mean}(\tilde{s}_{h,t}^q) + n_r \text{std}(\tilde{s}_{h,t}^q)} \tag{9}$$

respectively.

The *modified DI* is defined to be

$$DI_t^q := \left\| \begin{bmatrix} F_{r,t}^q \\ C_{r,t}^q \\ F_{r,t}^q C_{r,t}^q \end{bmatrix} \right\|^2 \tag{10}$$

where $C_{r,t}^q$ takes the larger value between $M_{r,t}^q$ and $S_{r,t}^q$, and $\|\cdot\|^2$ denotes the Euclidian vector norm.

The CD, which is derived based on the multivariate T^2 statistic, is used to quantify the similarity between the causal dependency of two variables under current operating conditions and historical operating conditions. When the CD is larger than the predefined threshold, the causal dependency of the two variables is broken. The CD requires a causal map containing the causal relationship between all of the measured variables, which can be derived based on knowledge from a plant engineer and the sample covariance matrix from the normal data.

For causal dependency, define c as the cause variable and e as the effect variable. The CD is based on the multivariable T^2 statistic, which is defined by

$$CD_{c,e} := T_{c,e}^2 = (\boldsymbol{y} - \bar{\boldsymbol{y}})^{\mathrm{T}} S_{c,e}^{-1} (\boldsymbol{y} - \bar{\boldsymbol{y}}) \tag{11}$$

where $\boldsymbol{y} = [\, c \quad e \,]^{\mathrm{T}}$, $\bar{\boldsymbol{y}}$ is the mean of $\boldsymbol{y}$, and $\boldsymbol{S}_{c,e}$ is the sample covariance for variables c and e.

Overall, the DI measure is used to detect a change in the frequency distribution for each measure variable, and the CD measure is utilized to detect a change in the causal relationship between two variables.

2.2. The proposed DI/CD based diagnosis method for multiple and unknown faults

The proposed approach based on the modified distance (DI) and modified causal dependency (CD) for the on-line diagnosis of multiple and unknown faults is illustrated in Fig. 2 and described in three steps: (1) The first step is to screen out the fault classes that are not associated with the on-line observations. (2) The second step determines the on-line observations to be associated with an unknown fault or known fault. (3) The last step classifies whether the on-line observations are related with a single fault or multiple faults. The steps are elaborated below.

Using the training set for Fault j, the fault propagation path (denoted by FP_j) is determined as the variables that satisfy

$$DI_t^q > DI_\alpha \tag{12}$$

and

$$T_{c,e}^2 > T_\alpha^2 \tag{13}$$

where DI_α and T_α^2 are the thresholds corresponding to the upper $100\alpha\%$ critical values which can be determined from the historical data.

The FP_j reveals the dynamics and the effects of Fault j on the variables. Such information is especially important to fault diagnosis, especially to diagnose multiple and unknown faults. Denote the variable with the highest DI as q^*. Similarly, denote the causal

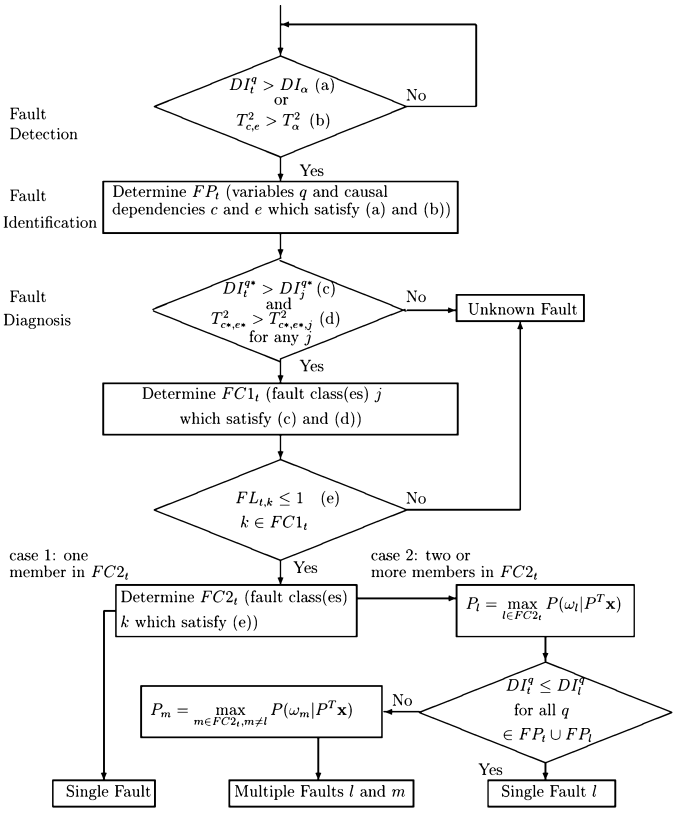

Fig. 2. Flowchart of the proposed DI/CD-based algorithm for detecting and diagnosing faults.

dependency c and e with the highest CD as c^* and e^*. The variable q^* and the causal dependency c^* and e^* are highly correlated with the root cause for Fault j. For on-line operation associated with Fault j, the magnitude for $DI_t^{q^*}$ and T_{c^*,e^*}^2 are expected to be high, relative to the rest of the variables. For each training set j, the upper bounds DI_j^q of the modified distance for each variable $q = 1$ to m is determined by the upper $100\alpha\%$ critical value of $\{DI_{t,l}^q \,|\, t = b, b+1, b+2, \cdots\}$, where $DI_{t,l}^q$ is calculated for time $t - b + 1$ to t (b is the moving window size). This information will be used to diagnose multiple faults.

The first step for on-line fault diagnosis is to screen out the fault classes that are not associated with the on-line observations. This step will increase the speed of diagnosis, which is especially important when the number of fault classes p in the historical database is large. With the above-mentioned off-line analysis, q^*, c^*, and e^* are obtained for each fault class. Then two conditions are checked for $j = 1$ to p:

$$DI_t^{q^*} > DI_j^{q^*} \tag{14}$$

$$CD_{c^*,e^*} > CD_{c^*,e^*,j} \tag{15}$$

where $DI_j^{q^*}$ is the pre-specified lower bound for variable q^* in Fault j, which is determined by the lower $100\alpha\%$ critical value of $\{DI_{t,j}^{q^*} \,|\, t = b, b+1, b+2, \cdots\}$; and $CD_{c^*,e^*,j}$ is the pre-specified lower bound for causal dependency c^* and e^* in Fault j, which is also determined by its lower $100\alpha\%$ critical value. Record all fault classes that satisfy (14) and (15), and denote such classes by $FC1_t$. These fault classes are potential fault candidates and further tests are required to diagnose the root cause. On-line observations that do not satisfy (14) and (15) are not associated with Fault j.

The second step of on-line fault diagnosis is to determine whether the on-line observations are associated with an unknown fault or known fault. The training sets associated with all the fault

candidates are used for this purpose. For fault class $j \in FC1_t$, the modified DI for each element q in $FP_t \cap FP_j$ is computed by (10) as $DI^q_{t,j}$.

The fault likelihood is then calculated as

$$FL_{t,j} = \frac{1}{N_{DI}} \sum_{q}^{N_{DI}} \frac{DI^q_{t,j}}{DI_\alpha} \tag{16}$$

where N_{DI} is the number of elements in $FP_t \cap FP_j$.

It is likely that the on-line observations are associated with Fault j when $FL_{t,j} \leq 1$. Record all fault classes k in which $FL_{t,k} \leq 1$ and denote such classes by $FC2_t$. These fault classes are potential fault candidates and further tests are required to diagnose the root cause. Fault classes in which $FL_{t,k} > 1$ are not responsible for the out-of-control operations.

The final step of on-line diagnosis is to determine whether the on-line observations are associated with a single fault or multiple faults. If there is only one fault candidate in $FC2_t$, denoted by l, then this single Fault l is responsible for the abnormal situation.

If there are more than one fault candidate in $FC2_t$, the most probable fault class can be determined using Bayes' rule and PCA. Bayes' rule can discriminate observations associated with known classes, but it has no ability to discriminate observations associated with unknown classes. Once the fault likelihood (16) has been used to screen out the observations associated with unknown faults, the use of Bayes' rule and PCA can provide an accurate classification of the on-line observations.

For an observation projected onto the PCA dimensions, Bayes' rule is

$$p(\omega_l|\boldsymbol{P}^{\mathrm{T}}\boldsymbol{x}) = \frac{p(\boldsymbol{P}^{\mathrm{T}}\boldsymbol{x}|\omega_l)p(\omega_l)}{p(\boldsymbol{P}^{\mathrm{T}}\boldsymbol{x})} \tag{17}$$

where $\boldsymbol{P}^{\mathrm{T}}\boldsymbol{x}$ is the observation projected onto the PCA dimension, $p(\omega_l)$ is the a priori probability for Fault ω_l, $p(\boldsymbol{P}^{\mathrm{T}}\boldsymbol{x}|\omega_l)$ is the probability density function for $\boldsymbol{P}^{\mathrm{T}}\boldsymbol{x}$ conditioned on ω_l, and $p(\boldsymbol{P}^{\mathrm{T}}\boldsymbol{x})$ is the probability density function for $\boldsymbol{P}^{\mathrm{T}}\boldsymbol{x}$:

$$p(\boldsymbol{P}^{\mathrm{T}}\boldsymbol{x}) = \sum_{l=1}^{n_{FC2}} p(\boldsymbol{P}^{\mathrm{T}}\boldsymbol{x}|\omega_l)p(\omega_l) \tag{18}$$

where n_{FC2} is the number of fault candidates in $FC2_t$. If the data for each class are normally distributed, $p(\boldsymbol{P}^{\mathrm{T}}\boldsymbol{x}|\omega_l)$ is given by

$$p(\boldsymbol{P}^{\mathrm{T}}\boldsymbol{x}|\omega_l) = \frac{\exp\left[-\frac{1}{2}(\boldsymbol{x}-\boldsymbol{x}_l)^{\mathrm{T}}\boldsymbol{P}\left(\frac{1}{n_l-1}\boldsymbol{P}^{\mathrm{T}}\boldsymbol{S}_l\boldsymbol{P}\right)^{-1}\boldsymbol{P}^{\mathrm{T}}(\boldsymbol{x}-\boldsymbol{x}_l)\right]}{(2\pi)^{a/2}\left[\frac{1}{n_l-1}\det(\boldsymbol{P}^{\mathrm{T}}\boldsymbol{S}_l\boldsymbol{P})\right]^{1/2}} \tag{19}$$

where n_l in the number of observations in Fault l, $\boldsymbol{S}_l$ is the sample covariance of Fault l, a is the PCA dimensions, and $\boldsymbol{P}$ is the PCA projection.

With (17)–(19), $p(\omega_l|\boldsymbol{P}^{\mathrm{T}}\boldsymbol{x})$ can be determined for $l \in FC2_t$. The observations are assigned to the fault class l that maximizes $p(\omega_l|\boldsymbol{P}^{\mathrm{T}}\boldsymbol{x})$. To determine whether all the symptoms can be explained by fault class l, the condition

$$DI^q_t < DI^q_l \tag{20}$$

is checked for all variables $q \in FP_t \cup FP_l$. Recall that the upper bounds DI^q_l of the modified distance are determined by the upper $100\alpha\%$ critical value of $\{DI^q_{t,l} \,|\, t = b, b+1, b+2, \cdots\}$, where $DI^q_{t,l}$ is calculated for $t-b+1$ to t (b is the moving window size). If the condition holds, a single fault class l is determined. Otherwise, $p(\omega_l|\boldsymbol{P}^{\mathrm{T}}\boldsymbol{x})$ is determined for $m \in FC2_t$, where $m \neq l$. Both fault classes l and m are responsible for the out-of-control operations.

The framework of three steps mentioned above systematically utilizes a more complete set of feature representations of faults (including the data-driven, causal connectivity-based, and propagation path-based features). In particular, the second and third steps incorporate the propagation path-based feature representation of faults to check the variables $q \in FP_t \cap FP_j$ (Step 2) or $q \in FP_t \cup FP_l$ (Step 3), which significantly distinguishes the proposed approach from the most of existing hybrid methods which only utilize the data-driven and/or causal map-based features.

3. Case studies

3.1. Tennessee Eastman process

The Tennessee Eastman process [17] is a well-known benchmark for monitoring and control studies. A detailed description of the plant and associated faults is available elsewhere [3]. The process flowsheet and the process faults are shown in Fig. 3 and Table 1, respectively. In addition to the training set for Fault 0, which represents normal operating conditions, training sets for Faults 1–15 were generated. The total number of observations generated for each run was $n = 500$, where 480 observations were collected after the introduction of the fault. Only these 480 observations are actually used to construct the process monitoring measures. The same testing sets for Faults 0–21 were used. In addition, 105 different Tennessee Eastman plant simulation runs were obtained, each with 800 observations and different combinations of two faults from Fault 1–15.

3.2. Case studies

Several data sets from the Tennessee Eastman plant simulator are used to evaluate the proposed method for diagnosing faults.

Case Study on Fault 6. This case study is used to evaluate the performance of the proposed fault diagnosis algorithm for a fault in which pure data-driven methods fail. Fault 6 involves unsteady operations, in which most variables are affected. Consider the significance level $\alpha = 0.01$ and the moving window of observation number $b = 20$ for this case study. Consider the first 20 observations, i.e., 1 h after Fault 6 occurs. After checking the two conditions (14) and (15) in the first step of the fault diagnosis procedure, the fault class candidates associated with these on-line observations are $FC1_t = \{$Faults 4, 6, 11, and 14$\}$. The fault propagation path 1 h after Fault 6 occurs is depicted in Fig. 4. By examining the fault likelihood (16) of the second step of the fault diagnosis procedure, it can be further obtained that the observations are linked to known faults, and the fault class candidates $FC2_t = \{$Faults 4, 6, and 11$\}$. After the third step of using the fault candidates in $FC2_t$ to explain the symptoms, the observations are finally diagnosed as a single Fault 6. The rest of the observations are calculated similarly. The proposed DI/CD-based approach correctly diagnoses for 95.1% of the observations. Past work showed that the misclassification rate using purely data-driven algorithms range from 0.94 to 1 [15]. This case study indicates an advantage of the proposed DI/CD-based algorithm over the traditional data-based statistics for this very challenging fault.

Case Study for Independent Multiple Faults 4 and 5. This case study is used to evaluate the performance of the proposed fault diagnosis algorithm for *independent multiple faults*, in which individual fault has different effects on different variables. The effects of Faults 4 and 5 are to induce a step change in the reactor cooling water flow rate, and to induce a step change in the condenser cooling water flow rate, respectively. When Faults 4 and 5 occur simultaneously, Fault 4 affects the reactor cooling water flow rate, while Fault 5 affects the condenser cooling water flow rate. The modified distances for the reactor cooling water flow valve and the condenser cooling water flow valve for Fault 4, Fault 5, and multi-

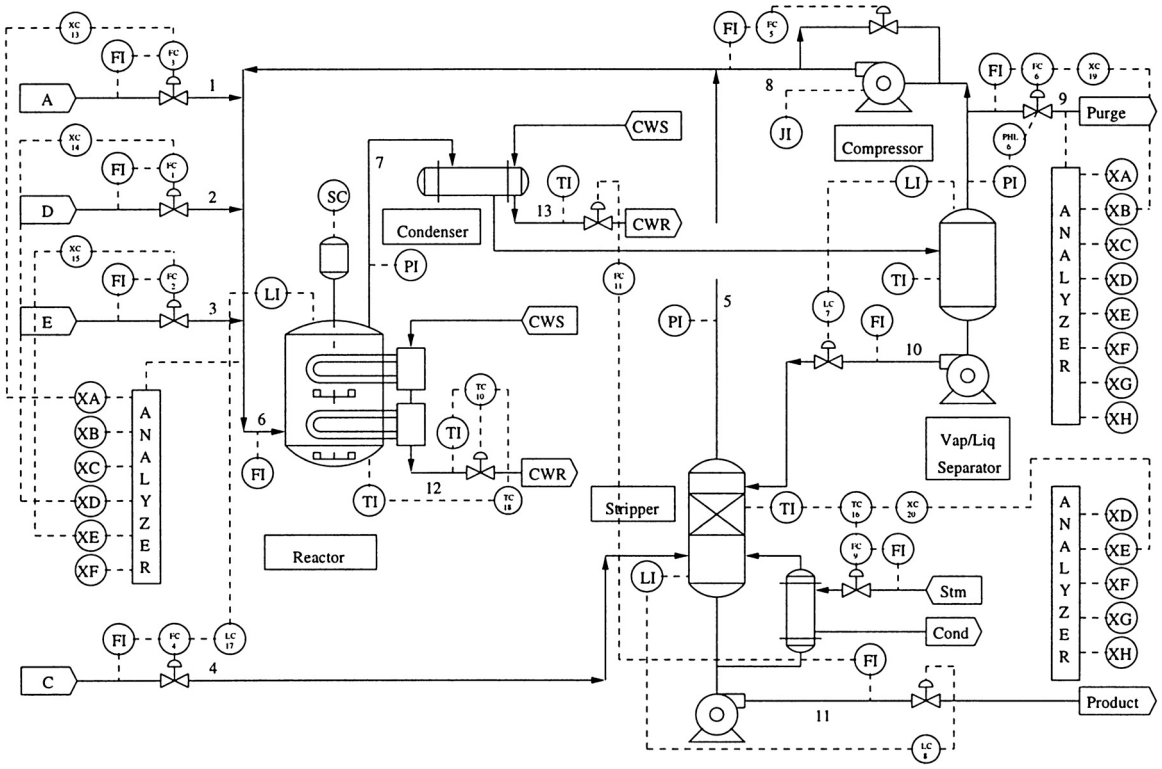

Fig. 3. A process flow diagram of the Tennessee Eastman problem.

Table 1
Process faults for the Tennessee Eastman process simulator.

Variable	Description	Type
IDV(1)	A/C Feed Ratio, B Composition Constant (Stream 4)	Step
IDV(2)	B Composition, A/C Ratio Constant (Stream 4)	Step
IDV(3)	D Feed Temperature (Stream 2)	Step
IDV(4)	Reactor Cooling Water Inlet Temperature	Step
IDV(5)	Condenser Cooling Water Inlet Temperature	Step
IDV(6)	A Feed Loss (Stream 1)	Step
IDV(7)	C Header Pressure Loss – Reduced Availability (Stream 4)	Step
IDV(8)	A, B, C Feed Composition (Stream 4)	Random Variation
IDV(9)	D Feed Temperature (Stream 2)	Random Variation
IDV(10)	C Feed Temperature (Stream 4)	Random Variation
IDV(11)	Reactor Cooling Water Inlet Temperature	Random Variation
IDV(12)	Condenser Cooling Water Inlet Temperature	Random Variation
IDV(13)	Reaction Kinetics	Slow Drift
IDV(14)	Reactor Cooling Water Valve	Sticking
IDV(15)	Condenser Cooling Water Valve	Sticking
IDV(16)	Unknown	
IDV(17)	Unknown	Constant Position
IDV(18)	Unknown	
IDV(19)	Unknown	
IDV(20)	Unknown	
IDV(21)	The valve for Stream 4 was fixed at the steady-state position	

ple Faults 4 and 5 are shown in Fig. 5. The modified distances of the reactor cooling water flow valve and the condenser cooling water flow valve for multiple Faults 4 and 5 are larger than the thresholds, indicating that the DI has detected abnormal behaviors in both variables.

Two disjointed fault propagation paths appear 15 min after multiple Faults 4 and 5 occur (see Fig. 6). The reactor cooling water flow valve has the highest ranking for one fault propagation path, while the separator cooling water outlet temperature had the highest ranking for the other fault propagation path. The reactor cooling water flow valve and the separator cooling water outlet temperature represent the root causes for Fault 4 and Fault 5, respectively.

The DI/CD algorithm successfully identifies the occurrence of the multiple faults for 91.4% of the time, while misdiagnosing the faults as a single fault or unknown faults for 4.9% and 3.8% of the time, respectively. Fault 4 is correctly identified as the contributing fault for 92.4% of the observations associated with multiple Faults 4 and 5, while Fault 5 is correctly diagnosed for 73.9% of the observations. The decentralized nature of the proposed algorithm suggests that accurate diagnosis would be expected for most independent multiple faults when the faults are within known fault classes.

Case Study for Dependent Multiple Faults 5 and 7. This case study is used to evaluate the performance of the proposed fault diagnosis algorithm for *dependent multiple faults*. Fault 7 involves a pressure loss in the *C* Header in Stream 4. As a result, the availabil-

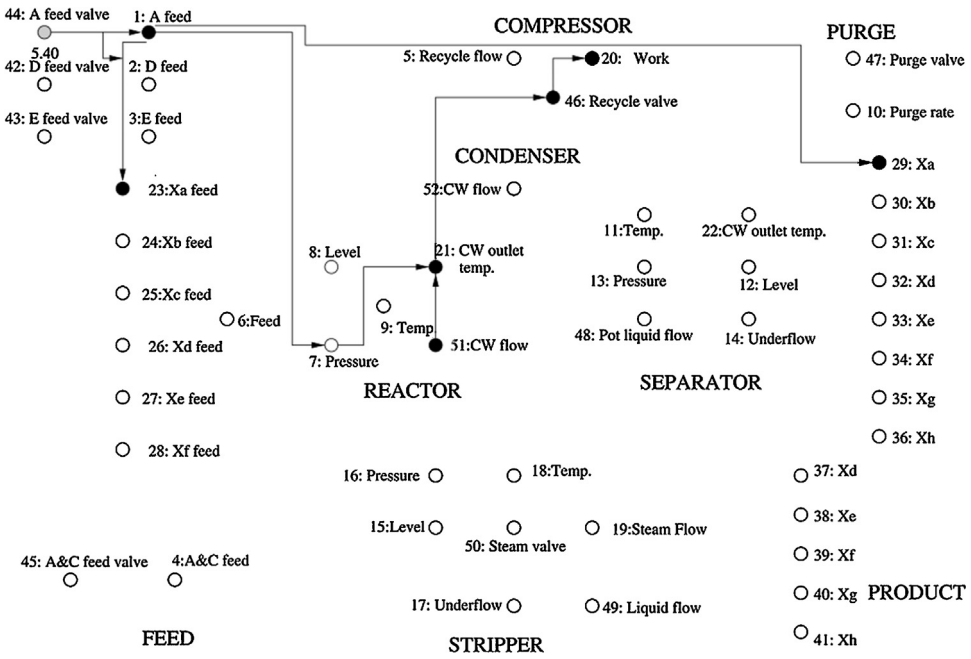

Fig. 4. Fault propagation path at $t = 9$ h (1 h after Fault 6 occurs). The variable with the highest DI is shown as a gray node, the broken variables are shown as black nodes, and broken causal dependencies are shown as vectors between nodes.

ity of component C in Stream 4 reduces and the total feed flow in Stream 4 decreases, which causes the control loop for Stream 4 to increase the valve for the total feed flow (see Fig. 7). After 20 h, the control loop is able to compensate for the change and the total feed remains at the desired level, while the valve for the total feed settles for a higher value. For the rest of the 50 variables that are monitored, 38 variables have similar transients that settle in about 15 h. The significant effect of Fault 5 is on the condenser cooling water valve (see Fig. 7). The total feed flow valve, the total feed flow in Stream 4, and other 30 variables have similar transients that settle in about 8 h (see Fig. 7). When Faults 5 and 7 occur simultaneously, the total feed flow valve and the condenser cooling water valve settle to new levels (see Fig. 7), while about 40 variables behave similarly as the total feed flow in Stream 4.

In this case study, the individual faults have similar effects on some common variables. The modified distances for the total feed

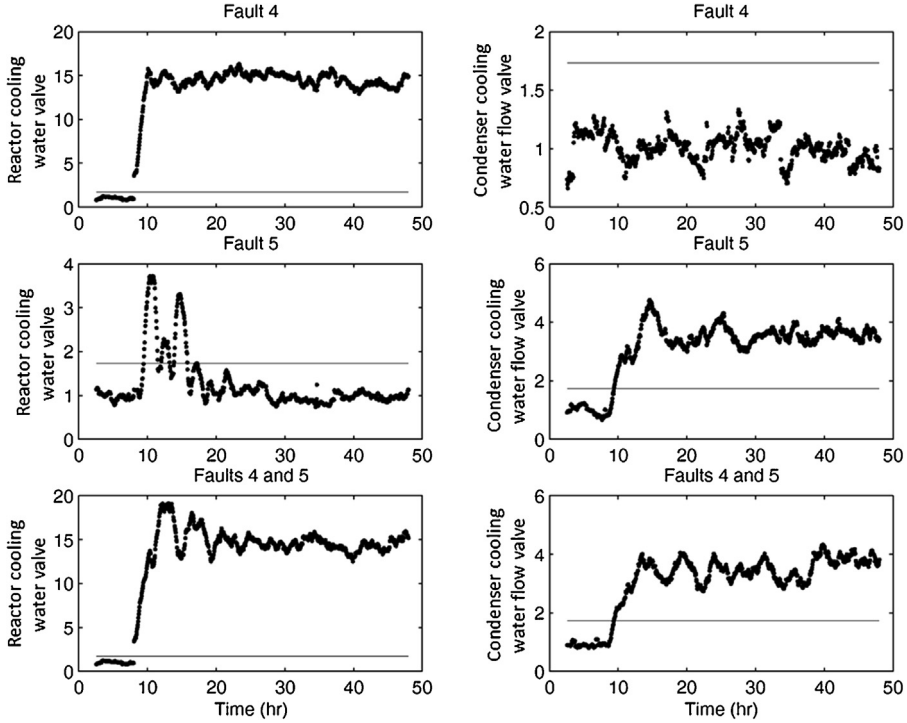

Fig. 5. The modified distances for the reactor cooling water valve and the condenser cooling water flow valve for Fault 4, Fault 5, and multiple Faults 4 and 5. The faults occur at $t = 8$ h. The solid line is the threshold.

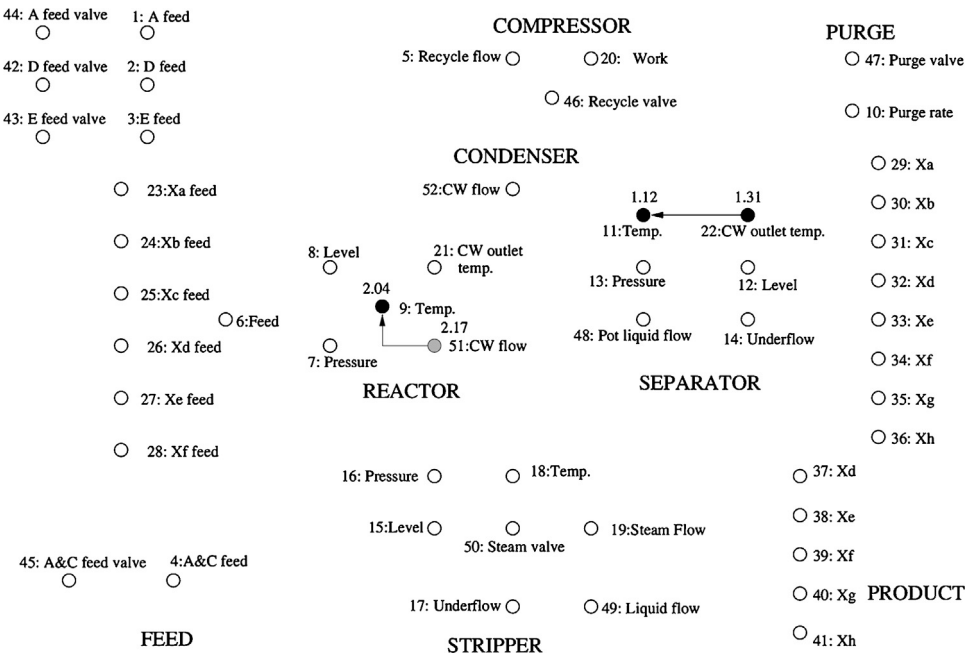

Fig. 6. Fault propagation path at $t = 8.25$ h (15 min after multiple Faults 4 and 5 occur). The variable with the highest DI is shown as a gray node, the broken variables are shown as black nodes, and broken causal dependencies are shown as vectors between nodes.

flow valve and the condenser cooling water flow valve for Fault 5, Fault 7, and multiple Faults 5 and 7 are shown in Fig. 8. The modified distances for the total feed flow valve and the condenser cooling water flow valve for multiple Faults 5 and 7 are larger than the thresholds, indicating that the DI has detected abnormal behaviors in both variables. The effect of Fault 5 on the total feed flow valve is masked by the dominating effect of Fault 7. The similar effects of Faults 5 and 7 on the total feed flow rate in Stream 4 and the separator cooling water outlet temperature are shown in Fig. 9.

The fault propagation path contains 8 variables 15 min after multiple Faults 5 and 7 occur (see Fig. 10). These variables reflect the symptoms for Fault 7, but not for Fault 5. One hour after mul-

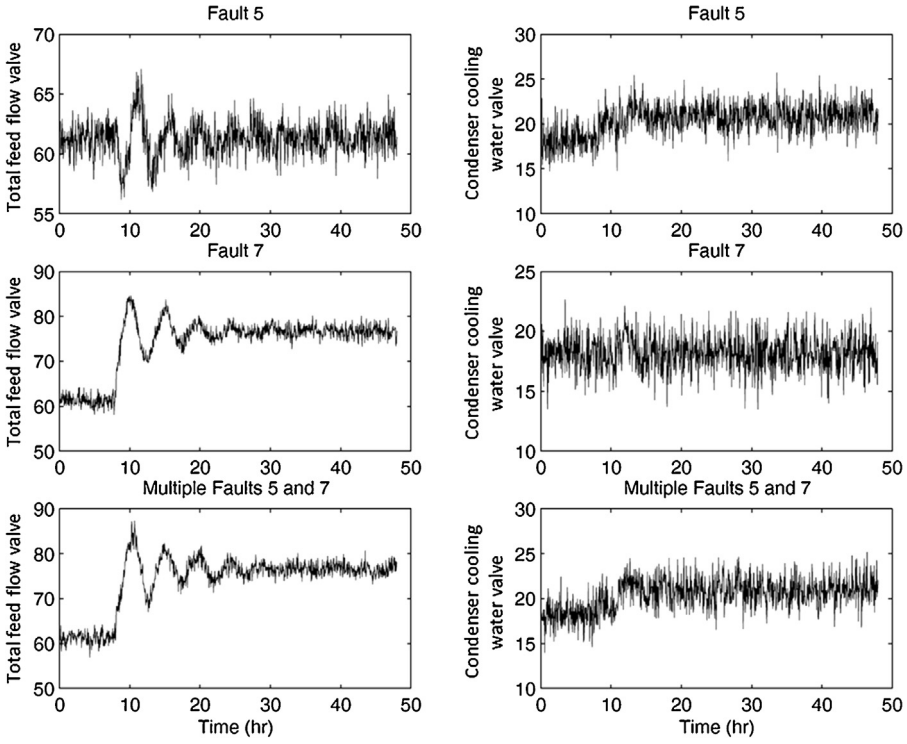

Fig. 7. Comparison of the total feed flow valve and the condenser cooling water valve for Fault 5, Fault 7, and multiple Faults 5 and 7.

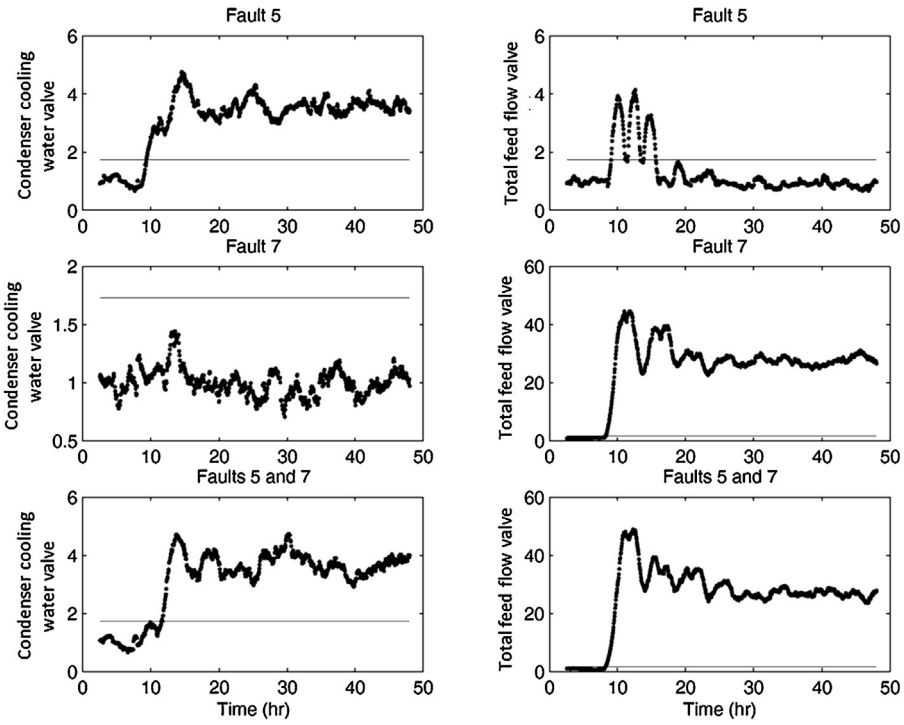

Fig. 8. The modified distances for the condenser cooling water valve and the total feed flow valve for Fault 5, Fault 7, and multiple Faults 5 and 7. The faults occur at $t = 8$ h. The solid line is the threshold.

tiple Faults 5 and 7 occur, the fault propagation path contains 32 variables, which include the symptoms for Faults 5 and 7.

The proposed DI/CD-based algorithm successfully identifies the occurrence of multiple faults for 97.4% of the time, while misdiagnosing the faults as a single fault for 2.0% of the time. Fault 5 is correctly identified as the contributing fault for 87.3% of the observations associated with multiple Faults 5 and 7, while Fault 7 is correctly diagnosed for 73.1% of the observations. The proposed algorithm is highly effective for this case study with multiple dependent faults.

Case Study for Masked Multiple Faults 4 and 6. Multiple Faults 4 and 6 are *masked multiple faults*, in which the variables affected by

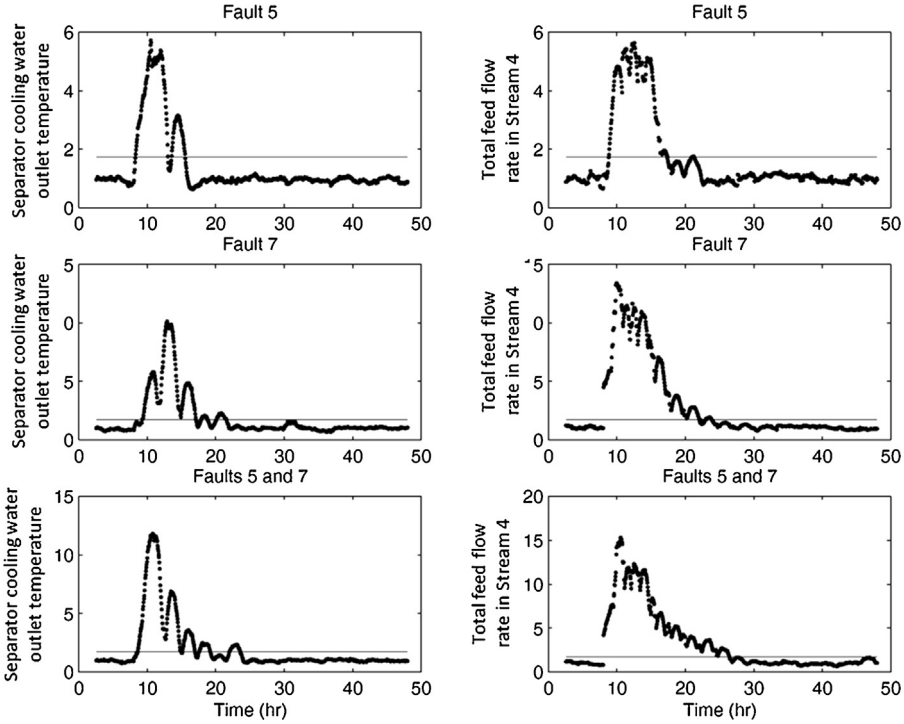

Fig. 9. The modified distances for the separator cooling water outlet temperature and the total feed flow rate in Stream 4 for Fault 5, Fault 7, and multiple Faults 5 and 7. The faults occur at $t = 8$ h. The solid line is the threshold.

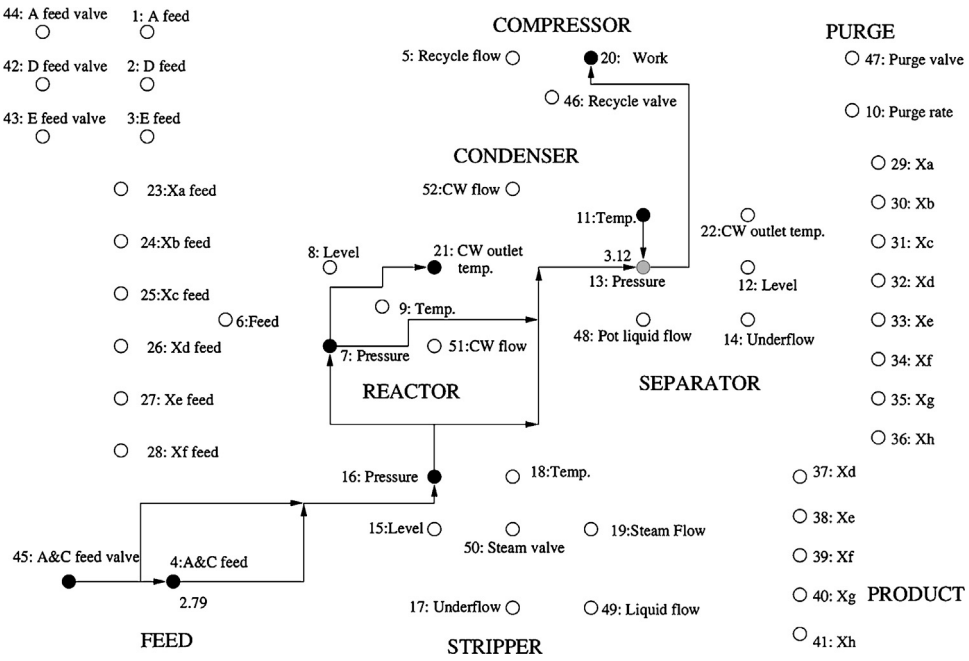

Fig. 10. Fault propagation path at $t = 8.25$ h (15 min after multiple Faults 5 and 7 occur). The variable with the highest DI is shown as a gray node, the broken variables are shown as black nodes, and broken causal dependencies are shown as vectors between nodes.

one fault are a subset of the variables affected by another fault. The above discussions show that Fault 6 involves unsteady operations, causing most variables to deviate significantly from their normal behaviors. Although Fault 4 has a clear effect on the reactor cooling water flow rate, the effect of Fault 4 is masked when both Faults 4 and 6 occur. As a result, only 9.4% of the observations are identified as associated with multiple faults, of which none of the observations are being diagnosed as Fault 4. On the other hand, 86.8% of the observations are identified as associated with a single fault, of which all of the observations are correctly diagnosed as Fault 6. Altogether, Fault 6 is diagnosed as the cause for 94.5% of the total observations. The proposed algorithm diagnoses the dominating fault for this case of masked multiple faults.

Case Study for Masked Multiple Faults 11 and 14. As a result of a sticking reactor cooling water valve in Fault 14, the reactor cooling water outlet temperature fluctuates around its set point. The large variability induced by Fault 14 causes the reactor temperature and the reactor cooling water flow to fluctuate as well (see Fig. 11). Fault 11 induces a random variation in the reactor cooling water inlet temperature. As a result, larger fluctuations in the reactor temperature and the reactor cooling water flow rate are observed. When multiple Faults 11 and 14 occur, Fault 11 is masked by Fault 14. Unlike masked multiple Faults 4 and 6, neither Fault 11 or 14 has a dominating effect over the other fault. It is interesting to observe that the magnitudes of the reactor cooling water flow rate and the reactor temperature for multiple faults 11 and 14 are larger than their magnitudes for single Fault 11 and Fault 14.

When Fault 11 occurs, the largest modified distances for the reactor temperature and the reactor cooling water flow rate are 16 and 27, respectively (see Fig. 12). When Fault 14 occurs, the largest modified distance for the reactor temperature and the reactor cooling water flow are 40 and 38, respectively (see Fig. 12). These values are significantly larger than the threshold, which is a strong indication that the reactor temperature and the reactor cooling water flow rate behave abnormally. However, these modified distances are smaller than the values associated with the multiple Faults 11 and 14, which are 79 and 70, respectively (see Fig. 12). Because of the significant difference between the modified distances for Fault 11, Fault 14, and multiple Faults 11 and 14, individual faults are not diagnosed when multiple Faults 11 and 14 occur. Instead, 99% of the observations are diagnosed as unknown faults. In this case, the fault propagation path shows abnormal behaviors in the reactor temperature and the reactor cooling water flow rate (see Fig. 13). These faults are isolated in the reactor area correctly.

3.3. Diagnosis of all known and unknown faults

This section compares the fault diagnosis proficiency for all 21 faults in the Tennessee Eastman Problem [3]. It is observed in Fig. 14 that the proficiency of proposed DI/CD-based approach for diagnosing unknown faults do not depend on order selection, because no order selection step is involved in diagnosing unknown faults (see Fig. 2). Fig. 14 shows that the proficiency of proposed algorithm for diagnosing known faults depends weakly on order selection, which indicates that the modified distance screens out a lot of fault candidates before using PCA and Bayes' rule to determine the most probable fault class in the final step of the algorithm.

The overall misclassification rate for the known Faults 0–15 using the proposed DI/CD-based method is about 0.26 for $a > 35$. When the unobservable Faults 3, 9, and 15 are not considered, the overall misclassification rate drops to 0.096. The modified distance depends on the recent distribution of the variables, which results in a detection delay. Considering the overall missed detection rate of 0.029 and the unavoidable detection delay, an overall misclassification rate of 0.096 is nearly perfect fault diagnosis.

3.4. Diagnosis of 225 sets of multiple faults

Table 2 shows the classification ratios for the individual faults in the testing sets associated with the multiple faults using the proposed DI/CD-based algorithm. For example, the first two numbers 0.932 and 0.767 in the column titled "4" indicate that, when Faults 1 and 4 occur simultaneously, the classification ratios for Faults 1 and 4 are 0.932 and 0.767, respectively.

When multiple faults occur with one of the individual faults being Faults 3, 9, and 15, the classification ratio for the other individual fault is very similar to the classification ratio when that

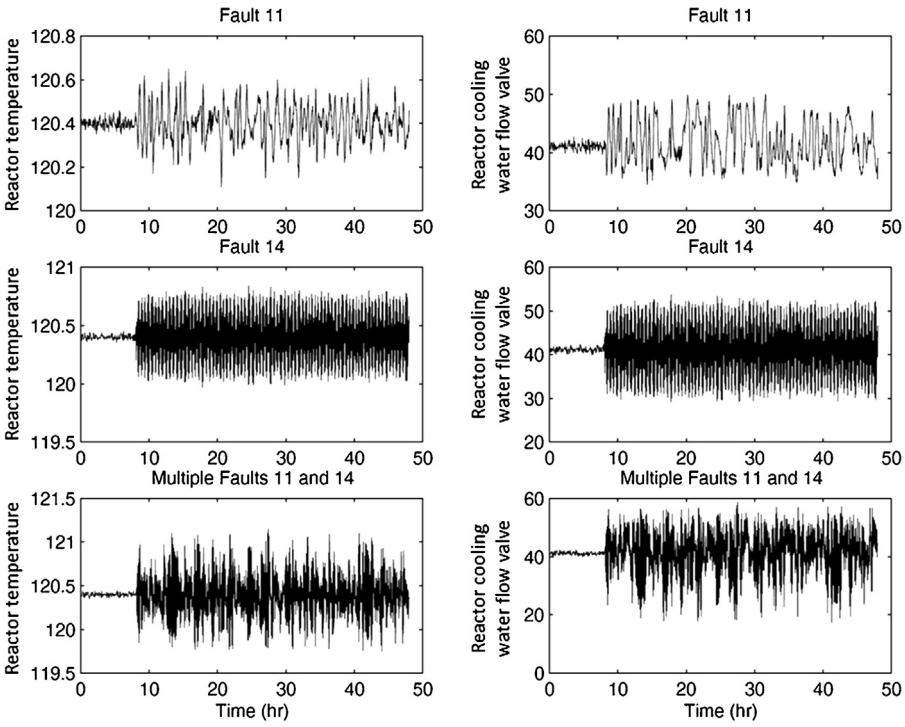

Fig. 11. Comparison of the reactor temperature and the reactor cooling water flow valve for Fault 11, Fault 14, and multiple Faults 11 and 14. The faults occur at $t = 8$ h.

individual fault occurs alone. For example, when Faults 2 and 3 occur simultaneously, the classification ratio for Fault 2 is 0.951, compared to 0.955 when Fault 2 occurs alone. This observation provides further confirmation that Faults 3, 9, and 15 are unobservable, indicating that the data for Fault 0 (normal operating conditions) and Faults 3, 9, and 15 are similar for all of the variables.

When multiple faults occur with one of the individual faults being Fault 6, the classification ratio for Fault 6 is high (>0.95) for almost all cases. Fault 6 affects 48 variables, of which 40 of the variables are severely affected. Fault 6 masked all other faults, which makes it very difficult to diagnose the other individual fault when these faults occur simultaneously.

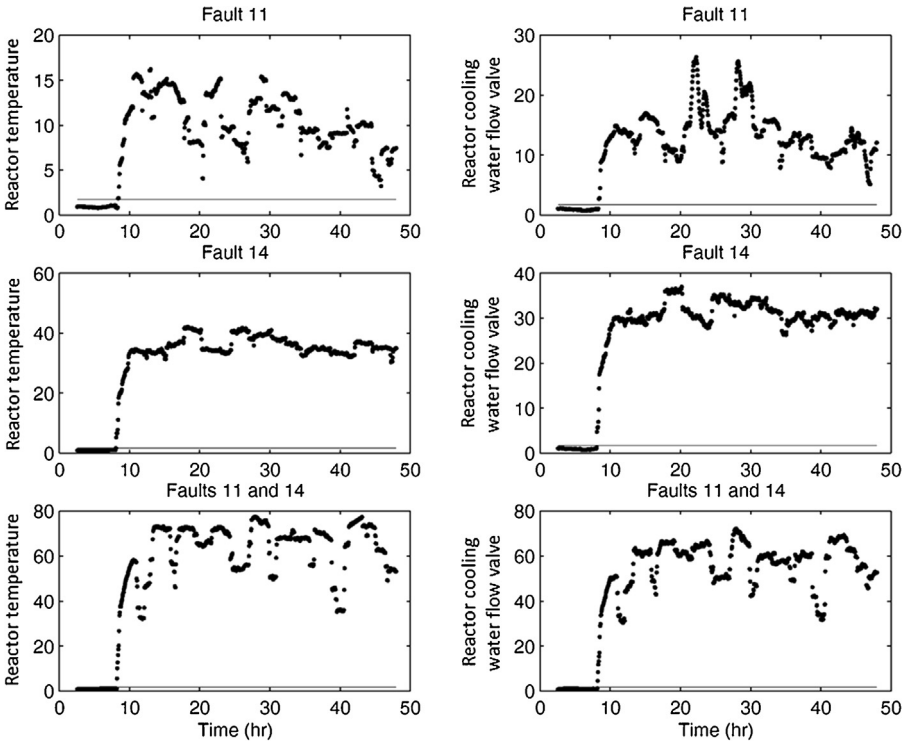

Fig. 12. The modified distances for the reactor temperature and the reactor cooling water flow valve for Fault 11, Fault 14, and multiple Faults 11 and 14. The faults occur at $t = 8$ h. The solid line is the threshold.

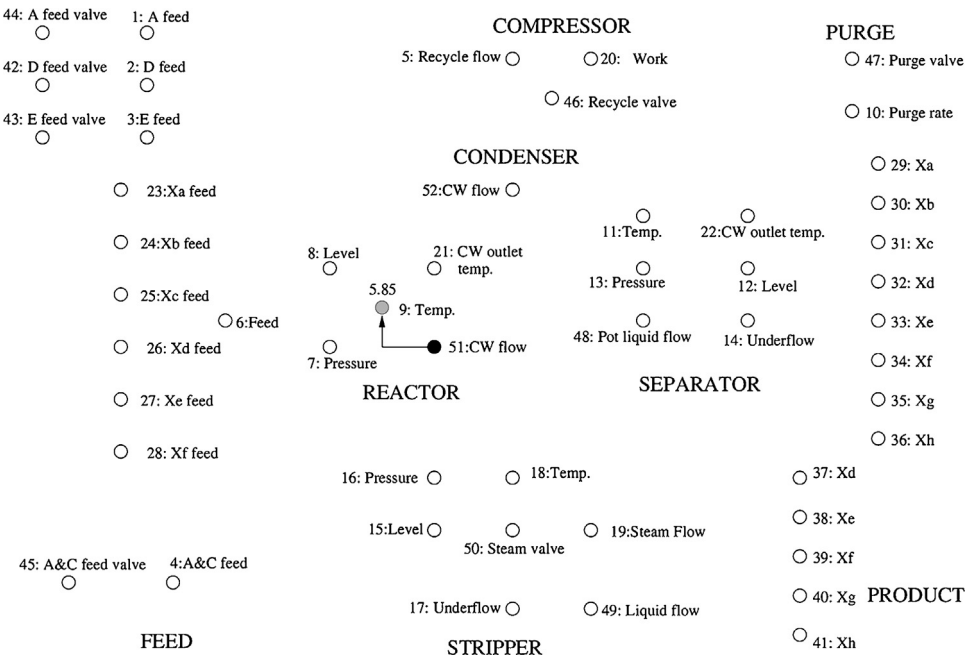

Fig. 13. Fault propagation path at $t = 8.25$ h (15 min after multiple Faults 11 and 14 occur). The variable with the highest DI is shown as a gray node, the broken variables are shown as black nodes, and broken causal dependencies are shown as vectors between nodes.

Overall, the proposed algorithm performed well for diagnosing multiple faults. For multiple faults with observable individual faults, at least one fault is diagnosed (i.e., classification ratio is greater than 0.85) for over half of the cases. For 92% of the cases, the classification ratio for at least one fault is greater than 0.5. For multiple faults where the classification ratios for the individual faults are less than 0.5 (i.e., Faults 1 and 12, Faults 4 and 14, Faults 6 and 7, Faults 11 and 14, Faults 12 and 13, Faults 13 and 14), most observations are diagnosed as being associated with unknown faults (see Table 3).

When multiple faults occur with known individual faults, they are seldom diagnosed as being associated with unknown faults. In other words, when both multiple faults are correctly diagnosed (that is, both numbers within a box in Table 2 are near one, such as for Faults 1 and 5), then the corresponding classification ratio of unknown faults is low (Table 3). A low classification ratio of unknown faults in Table 3 does not necessarily imply that both

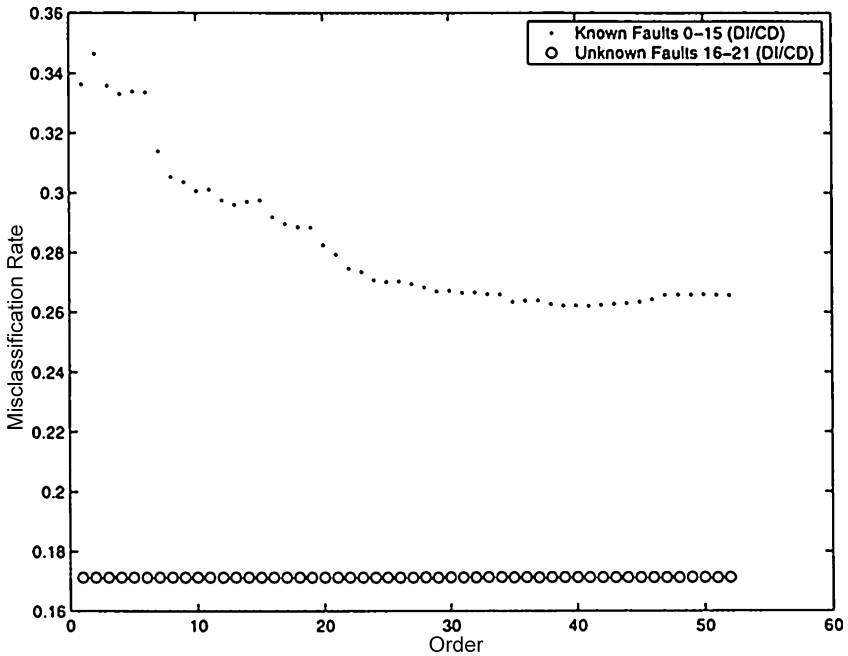

Fig. 14. The overall misclassification rates for the testing sets using DI/CD (models derived based on the training sets for Faults 0 to 15, each training set contains 480 observations).

Table 2
The classification ratios of the individual faults in the testing sets associated with the multiple faults using the proposed DI/CD-based method.

Fault	1	2	3	4	5	6	7	8	9	10	11	12	13	14	15
1	0.932	0.057	0.930	0.932	0.889	0.056	0.920	0.815	0.926	0.925	0.930	0.067	0.450	0.929	0.934
	–	0.850	0	0.767	0.944	0.974	0.151	0.591	0	0.005	0.651	0.230	0.541	0.766	0
2	0.850	0.955	0.951	0.950	0.775	0.010	0.859	0.936	0.951	0.952	0.947	0.741	0.734	0.947	0.954
	0.057	–	0	0.056	0.044	0.952	0.004	0.754	0	0	0.117	0.026	0.246	0.115	0
3	0	0	0	0	0	0	0	0	0	0	0	0	0	0	0
	0.930	0.951	–	0.921	0.886	0.954	0.936	0.730	0	0.709	0.939	0.779	0.931	0.982	0
4	0.767	0.056	0	0.916	0.739	0	0.731	0.110	0.914	0.916	0	0.004	0.015	0	0.912
	0.932	0.950	0.921	–	0.924	0.945	0.935	0.719	0	0	0.979	0.910	0.815	0	0
5	0.944	0.044	0.886	0.924	0.945	0	0.895	0.846	0.922	0.912	0.929	0.436	0.785	0	0.947
	0.889	0.775	0	0.739	–	0.961	0.709	0.201	0	0.630	0.774	0.594	0.506	0.931	0
6	0.974	0.952	0.954	0.945	0.961	0.951	0.466	0.956	0.946	0.945	0.947	0.965	0.956	0.977	0.951
	0.056	0.010	0.010	0	0	–	0	0.001	0	0	0	0	0	0.002	0
7	0.151	0.004	0.936	0.935	0.709	0	0.934	0.535	0.934	0.926	0.934	0.392	0.485	0.906	0.934
	0.920	0.859	0	0.731	0.895	0.466	–	0.901	0	0.072	0.716	0.934	0.880	0.787	0
8	0.591	0.754	0.730	0.719	0.201	0.001	0.901	0.799	0.524	0.756	0.669	0.589	0.954	0.591	0.770
	0.815	0.936	0	0.110	0.846	0.956	0.535	–	0	0.117	0.276	0.631	0.624	0.560	0
9	0	0	0	0	0	0	0	0	0	0	0	0	0	0	0
	0.926	0.951	0	0.914	0.922	0.946	0.934	0.524	–	0.624	0.845	0.647	0.916	0.965	0
10	0	0	0.709	0	0.630	0	0.072	0.117	0.624	0.664	0.032	0.112	0.136	0	0.746
	0.926	0.951	0	0.916	0.912	0.945	0.926	0.756	0	–	0.902	0.840	0.754	0.995	0
11	0.651	0.117	0.939	0.979	0.774	0	0.716	0.276	0.845	0.902	0.964	0.047	0.132	0.007	0.932
	0.930	0.947	0	0	0.929	0.947	0.934	0.669	0	0.032	–	0.906	0.854	0.004	0
12	0.230	0.026	0.779	0.910	0.594	0	0.934	0.631	0.647	0.840	0.906	0.889	0.147	0.726	0.856
	0.067	0.741	0	0.004	0.436	0.965	0.392	0.589	0	0.112	0.047	–	0.147	0.075	0
13	0.541	0.246	0.931	0.815	0.506	0	0.880	0.624	0.916	0.754	0.854	0.147	0.666	0.447	0.807
	0.450	0.734	0	0.015	0.785	0.956	0.485	0.954	0	0.136	0.132	0.147	–	0.064	0
14	0.766	0.115	0.982	0	0.931	0.002	0.787	0.560	0.965	0.995	0.004	0.075	0.064	0.966	0.959
	0.929	0.947	0	0	0	0.977	0.906	0.591	0	0	0.007	0.726	0.447	–	0
15	0	0	0	0	0	0	0	0	0	0	0	0	0	0	0
	0.934	0.954	0	0.912	0.947	0.951	0.934	0.770	0	0.746	0.932	0.856	0.807	0.959	–

Table 3
The classification ratios of the unknown faults in the testing sets associated with the multiple faults using the proposed DI/CD-based method.

Fault	1	2	3	4	5	6	7	8	9	10	11	12	13	14	15
1	0	0.017	0.023	0.024	0.028	0.023	0.023	0.123	0.020	0.021	0.021	0.679	0.020	0.006	0.025
2	0.017	0	0.036	0.050	0.043	0.039	0.004	0.033	0.039	0.038	0.011	0.038	0.031	0.008	0.031
3	0.023	0.036	0	0.076	0.043	0.039	0.005	0.165	0.194	0.253	0.060	0.073	0.012	0.008	0.244
4	0.024	0.050	0.076	0	0.038	0.039	0.005	0.126	0.086	0.084	0.021	0.033	0.080	0.952	0.074
5	0.028	0.043	0.043	0.038	0	0.036	0.006	0.059	0.055	0.043	0.028	0.315	0.048	0.015	0.048
6	0.023	0.039	0.039	0.039	0.036	0	0.517	0.039	0.040	0.041	0.041	0.035	0.040	0.010	0.039
7	0.023	0.004	0.005	0.005	0.006	0.517	0	0.008	0.004	0.005	0.005	0.005	0.005	0.009	0.005
8	0.123	0.033	0.165	0.126	0.059	0.039	0.008	0	0.311	0.106	0.105	0.129	0.016	0.005	0.153
9	0.020	0.039	0.194	0.086	0.055	0.040	0.004	0.311	0	0.336	0.148	0.095	0.029	0.025	0.198
10	0.021	0.038	0.253	0.084	0.043	0.041	0.005	0.106	0.336	0	0.084	0.055	0.109	0.003	0.224
11	0.021	0.011	0.060	0.021	0.028	0.041	0.005	0.105	0.148	0.084	0	0.006	0.005	0.990	0.060
12	0.679	0.038	0.073	0.033	0.315	0.035	0.005	0.129	0.095	0.055	0.006	0	0.756	0.005	0.058
13	0.020	0.031	0.012	0.080	0.048	0.040	0.005	0.016	0.029	0.109	0.005	0.756	0	0.347	0.045
14	0.006	0.008	0.008	0.952	0.015	0.010	0.009	0.005	0.025	0.003	0.990	0.005	0.347	0	0.029
15	0.025	0.031	0.244	0.074	0.048	0.039	0.005	0.153	0.198	0.224	0.060	0.058	0.045	0.029	0

multiple faults are diagnosed. For example, the classification ratio of unknown fault is 0.023 for Faults 1 and 6 (Table 3) although only Fault 6 is well diagnosed (Table 2). For multiple Faults 1 and 6, the undiagnosed individual Fault 1 is classified as being other known faults rather than as unknown faults.

4. Conclusions

A three-step framework for fault diagnosis based on DI/CD measures was proposed and applied for diagnosing known, unknown, and multiple faults in the Tennessee Eastman process. A total of 16 known faults, 6 unknown faults, and 105 multiple faults cases were investigated. The proposed diagnosis algorithm correctly diagnosed the known and unknown faults for most observations. For independent multiple faults, the proposed approach diagnosed both of the individual faults. For dependent multiple faults, the algorithm diagnosed the dominating individual faults for most cases. Diagnosing masked multiple faults is the most challenging case as the symptoms of one fault are completed masked by another fault. If both faults contribute equally, the proposed DI/CD-based algorithm diagnosed the multiple faults as unknown faults. When one fault was dominating the other fault in the masked multiple faults, the proposed algorithm diagnosed the dominating fault.

Acknowledgment

This work was supported by International Paper and the National Center for Supercomputing Applications.

References

[1] R. Brunelli, T. Poggio, Face recognition: features versus templates, IEEE Trans. Pattern Anal. Mach. Intell. 15 (1993) 1042–1052.
[2] H. Jiang, R. Patwardhan, S.L. Shah, Root case diagnosis of plant-wide oscillations using the concept of the adjacency matrix, J. Process Control 19 (2009) 1347–1354.

[3] L.H. Chiang, E.L. Russell, R.D. Braatz, Fault Detection and Diagnosis in Industrial Systems, Springer Verlag, London, UK, 2001.
[4] S. Yoon, J.F. MacGregor, Statistical and causal model-based approaches to fault detection and isolation, AIChE J. 46 (2000) 1813–1824.
[5] R. Isermann, Supervision, fault-detection and fault-diagnosis methods: an introduction, Control Eng. Pract. 5 (1997) 639–652.
[6] A.C. Raich, A. Cinar, Multivariate statistical methods for monitoring continuous processes: assessment of discriminatory power disturbance models and diagnosis of multiple disturbances, Chemom. Intell. Lab. Syst. 30 (1995) 37–48.
[7] A.C. Raich, A. Cinar, Statistical process monitoring and disturbance diagnosis in multivariable continuous processes, AIChE J. 42 (1996) 995–1009.
[8] L.H. Chiang, E.L. Russell, R.D. Braatz, Fault diagnosis in chemical processes using Fisher discriminant analysis, discriminant partial least squares, and principal component analysis, Chemom. Intell. Lab. Syst. 50 (2000) 243–252.
[9] G. Lee, S.-O. Song, E.S. Yoon, Multiple-fault diagnosis based on system decomposition and dynamic PLS, Ind. Eng. Chem. Res. 42 (2003) 6145–6154.
[10] N.F. Thornhill, A. Horch, Advances and new directions in plant-wide disturbance detection and diagnosis, Control Eng. Pract. 15 (2007) 1196–1206.
[11] M. Bauer, J.W. Cox, M.H. Caveness, J.J. Downs, N.F. Thornhill, Finding the direction of disturbance propagation in a chemical process using transfer entropy, IEEE Trans. Control Syst. Technol. 15 (2007) 12–21.
[12] N.F. Thornhill, J.W. Cox, M.A. Paulonis, Diagnosis of plant-wide oscillation through data-driven analysis and process understanding, Control Eng. Pract. 11 (2003) 1481–1490.
[13] J. Thambirajah, L. Benabbas, M. Bauer, N.F. Thornhill, Cause-and-effect analysis in chemical processes utilizing XML, plant connectivity and quantitative process history, Comput. Chem. Eng. 33 (2009) 503–512.
[14] R.M. Cruz, G.D. Cavalcanti, I.R. Tsang, R. Sabourin, Feature representation selection based on Classifier Projection Space and Oracle analysis, Expert Syst. Appl. 40 (2013) 3813–3827.
[15] L.H. Chiang, Fault Detection and Diagnosis for Large-scale Systems (Ph.D. Thesis), University of Illinois, Urbana, IL, 2001.
[16] L.H. Chiang, R.D. Braatz, Process monitoring using causal map and multivariate statistics: fault detection and identification, Chemom. Intell. Lab. Syst. 65 (2003) 159–178.
[17] J.J. Downs, E.F. Vogel, A plant-wide industrial process control problem, Comput. Chem. Eng. 17 (1993) 245–255.